Supporting Information

Elucidating the Role of Oxidation in Two-dimensional Silicon Nanosheets

Jeremy B. Essner,[a] Abhijit Bera,[a] Maharram Jabrayilov,[a] Abhishek Chaudhari,[a] Benjamin T. Diroll,[c] Julia V. Zaikina[b] and Matthew G. Panthani[a,*]

[a]Department of Chemical and Biological Engineering, Iowa State University, Ames, Iowa 50011, United States of America

[b]Department of Chemistry, Iowa State University, Ames, Iowa 50011, United States of America

[c]Center for Nanoscale Materials, Argonne National Laboratory, 9700 S. Cass Avenue, Lemont, IL 60639, United States of America

*Corresponding author email address: panthani@iastate.edu

Table of Contents

Experimental Details:

List of Figures:

List of Tables:

Experimental Methods

Materials

Calcium hydride (CaH_2; 98%) and silicon (99.9999%) were acquired from Alfa Aesar. Concentrated hydrochloric acid (A144C-212; Certified ACS Plus, 36.5 to 38.0%) and molecular sieves (M514; Type 4A; 8-12 Mesh Beads) were sourced from Fisher Scientific. Acetonitrile (271004; anhydrous, 99.8%), methanol (322415; anhydrous, 99.8%), and FTIR-grade mineral oil (M3516) were purchased from Millipore Sigma. All chemicals were used as received without further purification except the following: (i) the molecular sieves were extensively dried prior and all anhydrous acetonitrile and methanol employed in this work were degassed prior to use, unless otherwise noted.

Sample Preparation

$CaSi_2$ Synthesis

The silicon nanosheet, Zintl phase precursor, $CaSi_2$, was synthesized following our previously reported hydride approach.[1] Specifically, silicon lumps were ground to a fine powder in a Plattner's mortar & pestle. Then, in an argon-filled glovebox, quantities of CaH_2 and Si powders were massed (in a molar ratio of CaH_2:Si = 1:2) such that the reaction would yield approximately 2 g of $CaSi_2$. The powders were loaded into a polystyrene grinding vial equipped with a slip-on cap, which was then sealed inside two polypropylene bags under argon atmosphere, brought out of the glovebox, and ball-milled (8000M MIXER/MILL) for 30 min. After ball-milling, the CaH_2-Si mixture was returned to the glovebox and loaded in a Ta tube (Admat Inc., ~6-8" long, with 0.375" OD and 0.020" wall thickness), which was then welded shut using a gas tungsten arc welder and placed into a silica reactor. The reactor was evacuated down to 4×10^{-5} bar, placed in a resistance furnace (Thermo Scientific Thermolyne Type FD1500M) connected to thermo controllers (Eurotherm 3216), and heated at a rate of 2.03 °C min^{-1} from room temperature to 1000 °C, and held at 1000 °C for 24 hours. After 24 hours, the reactor was cooled to room temperature by switching off the furnace. The final product appeared as a fine black powder. The HS-$CaSi_2$ was stored in a glovebox under Ar or N_2 until needed.

Silicon Nanosheet Preparation

Note, all glassware described in the following sections underwent treatment in an alcoholic KOH bath prior to use, except for fritted filter glassware.

Conventional approach

In a glovebox filled with N_2, the synthesized $CaSi_2$ was massed in a vial and chilled to -35 °C under N_2 overnight. Prior to, Teflon tape was wrapped around the vial threads with at least three full wraps, and after filling with $CaSi_2$, at least three wraps of electrical tape were placed around the vial/cap interface, both to minimize potential air exposure. In a separate, three-neck, round-bottom flask, concentrated hydrochloric acid (HCl) was added. The outer necks were sealed with Suba-seal® septa (Chemglass; CG-3024), while the middle neck was sealed with a glass stopcock, flow control adaptor (Chemglass; CG-1028) for attachment to an Ar line. The flask was placed in the freezer and chilled to -35 °C under flowing Ar overnight. The next day, the pre-massed $CaSi_2$ was added to the flask under a continuous flow of Ar. For all deintercalations, the HCl:$CaSi_2$ mole ratio was kept constant at 116:1 (100 mL HCl per 1 gram $CaSi_2$) and glassware size/volume was adjusted accordingly. The reaction contents were allowed to sit unstirred at -35 °C for 10-14 days under positive Ar pressure, after which, the flask was removed from the freezer and the contents were vacuum filtered through a Buchner funnel (Chemglass; CG-8590; medium porosity) under flowing Ar, supplied by an inverted glass funnel that was suspended directly above the Buchner funnel. Once filtered, the funnel interface was thoroughly wrapped with Parafilm® and the entire filtration assembly was immediately transferred to a nitrogen-filled glovebox for further processing. The sample was then washed with degassed, anhydrous ACN at a ratio of ~100 mL ACN per gram of $CaSi_2$ deintercalated. After washing, the product was briefly dried on the filter (<5 min) before transferring to a vial for drying under vacuum for at least 24 h. The SiNSs were stored in a glovebox under N_2 atmosphere. Note, this sample may be referred to as "air-saturated HCl"; see below for sample nomenclature.

Oxygen-free approach

To generate SiNSs with minimal-to-no oxidation (assessed spectroscopically; see below), the steps taken were identical to those described in the "conventional approach" above except the HCl was first rigorously degassed before use and the manner in which the SiNSs were isolated was altered. To thoroughly degas the HCl, Ar gas was first bubbled through HCl for at least 24 h to purge oxygen. The HCl was then treated with four freeze-pump-thaw cycles on a Schlenk line. *Caution: conducting freeze-pump-thaw cycles on concentrated HCl is a dangerous process. Care should be taken to protect both the experimentalist and pump by employing defect-free glassware, ensuring the glassware volume is at least twice the volume of HCl, executing the freezing step slowly, and installing pre-pump traps (e.g., cold finger) to capture HCl vapors.* After the 4th thaw, the flask was charged with Ar, transferred to a -35 °C freezer, and treated similarly as described above. Once the reaction was complete, the flask was removed from the freezer and a septum was replaced with an Airfree® Schlenk fritted filter tube (Chemglass; AF-0544; medium porosity) under flowing Ar; a PTFE sleeve (Chemglass; CG-116) was employed in this joint connection. A flow control adaptor with a PTFE stopcock (Chemglass; CG-1031) was placed on the opposite end of the tube and a second, two-necked, round bottom flask was then attached to the other end of the flow control adaptor for collection of the HCl filtrate. A glass stopcock, flow control adaptor was placed in the other neck of the second, round bottom flask. The contents were then filtered through the fritted filter by carefully tilting the entire assembly such that the contents slowly flowed onto the filter and ensuring that the reaction contents did not come in contact with any vacuum grease. During the filtration process, the second flask was kept under vacuum while the initial reaction flask was kept under flowing Ar. Throughout the above steps, ground-glass joints were sealed with vacuum grease, unless otherwise noted, and all joints were wrapped with Teflon tape on the joint exterior, followed by plastic Keck clamps (Chemglass; CG-145). After filtration, all stopcocks were closed, the flask containing the HCl filtrate was removed, and the rest of the filtration assembly was transferred to a nitrogen-filled glovebox. The powder was removed from the filter and recollected in the initial reaction flask by filling the opposite end of the filter tube with degassed, anhydrous ACN and allowing the ACN to slowly permeate the filter until the entire sample was transferred to the flask. The ACN dispersion was then vacuum filtered again by transferring the contents to a Buchner funnel (Chemglass; CG-8590; medium porosity), followed by washing and drying, as described above. Note, this sample may be referred to as "degassed HCl"; see below for sample nomenclature.

Silicon Nanosheet Oxidation

To controllably oxidize the SiNSs, 10 mg mL^{-1} dispersions (~120 mg) were prepared in 40 mL vials with degassed, anhydrous ACN (~12 mL). To thoroughly seal the vials, (i) the threads had at least three wraps of Teflon tape around them, (ii) tightly fitting, sleeve-type septum stoppers (Chemglass; CG-3022) were employed in the cap hole instead of conventional TFE-lined silicone septa, and (iii) at least five full wraps of electrical tape were placed around the septum/vial interface. The headspace of the vials was evacuated by pumping on each vial for ~60 s through a syringe. Then incremental volumes of dry air (2.5, 5, 10, 20, or 40 mL) were injected in the vial headspace and the dispersions were magnetically stirred for 48 h. Lastly, the oxidized samples were dried under vacuum for at least 24 h and stored in a nitrogen-filled glovebox until needed. Note, the dry air employed was prepared by flowing air from an in-house line through a glass tube packed with molecular sieves and into a 1 L round bottom flask that also contained molecular sieves (~200 g). The outflow valve of the assembly was closed shortly before (~5 s) closing the inflow valve to achieve slight positive pressure within the assembly. The sieves in the air-filled flask were magnetically stirred for at least 24 h prior to use. The dry air was then extracted from the flask through a septum with a syringe and immediately injected into the vials. The nomenclature for these samples is described below.

Sample Nomenclature

All samples are described by the mole ratio of molecular oxygen that the SiNSs were intentionally exposed to relative to Si. These ratios are reported as parts per hundred (pph) O_2:Si, instead of pph, so as not to confuse readers with PL quantum yield values. To calculate this ratio for the sample prepared in air-saturated HCl, the solubility of O_2 in water at 0 °C (4.61E-4 mol L^{-1}) was converted to moles using the volume of HCl employed. This this value was ratioed to the moles of Si within the quantity of $CaSi_2$ precursor used in an individual deintercalation. To assess the pph of O_2 exposed to the SiNSs, the volume of O_2 in the aliquots of dried air added was calculated based on the known composition of air and this value was converted to moles using the Ideal Gas Law. For the purposes of this assessment, the SiNSs were assumed to consist completely of Si-H; the mass of SiNSs employed was converted to moles using the molecular weight of SiH. These two mole values were then ratioed. Also, for the purposes of this assessment, it was assumed that degassed HCl did not contain any molecular oxygen; in reality, trace levels are likely still present. The samples were then named as such, 0.0, 0.2, 0.5, 1.1, 2.2, 4.4, and 8.4 pph O_2 : Si, where these values equate to the degassed HCl sample, the air-saturated HCl sample, and SiNSs exposed to 2.5, 5, 10, 20, or 40 mL of dried air, respectively.

Sample Characterizations

Powder X-ray Diffraction (pXRD)

The purity of synthesized samples and identity of crystalline phases were confirmed by powder X-ray diffraction (pXRD) using a Rigaku MiniFlex600 powder diffractometer with Cu Kα radiation (λ = 1.54051 Å) and Ni Kβ filter. Data were collected on a zero-background plate holder in air. The raw .ras instrument files were converted to Excel (.xls) files for further processing using PowDLL Converter. All diffraction data were corrected for the signal originating from an empty sample holder and then baseline corrected with a spline curve, followed by normalization to the peak centered near $2\theta = 14°$. For the background correction, the diffraction signal across all 2θ values was uniformly scaled up or down to match the baseline of the empty sample holder between 2θ = 80-90°; the scaling factor was assessed by calculating the ratio of the average sample counts between 2θ = 80-90° to the average counts of the empty holder between 2θ = 80-90°. Additionally, the diffraction peaks in the 2θ range of 5-25° (d spacing of 17.7 to 3.6 Å) were deconvoluted to two components using the following linear combination of Gaussian and Lorentzian functions with different full-width at half maxima (see Figs. 1(A) and S5):

$$y = y_0 + A\left[m_u \frac{2}{\pi}\frac{w_L}{4(x - x_c)^2 + w_L^2} + (1 - m_u)\frac{\sqrt{4\ln 2}}{\sqrt{\pi}w_G} e^{-\frac{4\ln 2}{w_G^2}(x - x_c)^2}\right]$$

Scanning Electron Microscopy (SEM) and Energy-dispersive X-ray Spectroscopy (EDS)

SEM imaging and EDS were performed with an FEI Quanta 250 field-emission scanning electron microscope equipped with an Oxford Instruments X-Max 80 mm^2 silicon drift detector. The SEM images provided in this work were acquired via backscattered electrons. The contrast and brightness on all images were optimized in Adobe® Photoshop™ after acquisition. Samples were prepared in a glovebox filled with N_2 by either painting an aluminum SEM pin stub (Ted Pella, Inc., #16111) with carbon paint (Ted Pella, Inc., #16053) or affixing a double coated, high purity conductive carbon Spectro tab (Ted Pella, Inc., #16084-4) atop the pin stub, followed by sample deposition onto the carbon supports. In general, carbon tabs were employed for EDS while the carbon paint was employed for acquiring high-resolution images. To prepare samples for analysis, a small quantity (approximately 5–10 mg) of dried SiNS sample was placed on a sheet of weighing paper and uniformly spread out across an area of roughly 1.5 cm^2. The carbon covered pin stub was then carefully pressed against the sample (in the case of the carbon paint, while the paint was still wet) until the desired level of sample coverage was achieved. The sample-coated stubs were tapped against the weighing paper to knock off any poorly adhered SiNSs and also blown off with compressed air prior to loading to remove any loosely adhered SiNSs. The prepared stubs were either loaded into vials or an air-free holder, as described below.

For EDS analyses, an air-free stub holder (designed by ISU's MARL and fabricated by an on-campus machine shop) was employed to avoid the short air exposure (<10 min) upon sample loading. The prepared stubs were mounted in the holder, which was then pumped down to a pressure of 27 in Hg with a hand pump and placed in a glass mason jar that was sealed under N_2 atmosphere. The holder and jar were kept in a glovebox until transport to the SEM facility. The instrument was operated at an electron accelerating voltage of 10 kV and the samples were characterized in high vacuum mode. Both targeted-area spectra and elemental mapping were acquired with acquisition times of 30 s and approximately 10 min, respectively. All EDS data were initially processed with Oxford Instruments AZtec software prior to conducting statistical analyses and plotting.

For sample imaging, the prepared stubs were transferred to separate glass vials with an SEM pin mount gripper. To minimize potential oxygen exposure during transportation to the characterization facility, the threads of the vials were wrapped with at least three full rotations of PTFE plumber's tape prior to capping while, after capping, three full rotations of electrical tape were wrapped around the cap/vial interface. For samples deposited in carbon paint, the paint was allowed to dry before sealing the stub in a vial. The sample-loaded vials were kept in the glovebox until needed and the prepared stubs in the N_2-filled vials until immediately before loading into the SEM. During the loading and instrument preparation process, samples were exposed to air for no more than 10 min. The instrument was operated at an electron accelerating voltage of 10 kV and the samples were characterized in low vacuum mode with a water vapor pressure of 40–60 Pa to minimize charging effects.

Fourier-transform Infrared Spectroscopy (FTIR)

FTIR spectra were collected with a Nicolet iS5 FTIR spectrometer equipped with an iD7 Attenuated Total Reflectance (ATR) accessory. For all measurements, the employed crystal was diamond and the angle of incidence was 45°. The acquired spectra were an average of 64 scans across the wavenumber range of 4000-400 cm^{-1} with a spectral resolution of 8 cm^{-1}. To ensure that the SiNS samples prepared in degassed HCl were minimally exposed to oxygen, these samples were immersed in mineral oil (>100 mg mL^{-1}) in a nitrogen-filled glovebox prior to data collection, in addition to data collection of powdered samples in open air, for comparison. All FTIR data were baseline corrected using a spline curve and were normalized to the Si_3Si-H stretch centered near 2100 cm^{-1}.

Room Temperature Steady-state Photoluminescence

Steady-state photoluminescence spectra were acquired with both an OceanOptics JAZ and a PerkinElmer LS55 Fluorescence Spectrometer. The OceanOptics JAZ employed a 385 nm LED (ThorLabs; M385FP1) powered by a ThorLabs T-Cube LED driver (LEDD1B) as the excitation source which was coupled to OceanOptics UV-Visible optical fibers (QP400-2-UV-VIS or QP600-2-UV-VIS); the same fibers were employed for directing sample PL to the JAZ unit. The detectable wavelength range was 340–1020 nm (interval of ~0.4 nm) and counts were integrated for 3-5 s. For emission spectra collected on the PerkinElmer LS55, samples were excited at 359 nm and the PL was monitored from 370-900 nm, while excitation spectra were collected from 300-540 nm, monitoring PL at 550 nm, both at intervals of 0.5 nm. The excitation and emission slits were set at 10 nm and a built-in 10%T neutral density filter was employed.

In general, for acquisition of steady-state spectra, 0.1-0.5 mg mL^{-1} SiNS dispersions in ACN (or MeOH) were employed. The dispersions were prepared from stock solutions (typically, 4 mg mL^{-1}) that had been bath sonicated in an ice bath for at least 1 h prior to dilution and characterization. To minimize potential oxygen exposure during sonication, the threads of the vials were wrapped with at least three full rotations of PTFE plumber's tape prior to capping while, after capping, three full rotations of electrical tape were wrapped around the cap/vial interface. The dispersions were placed in Spectrocell Far UV Range threaded-top quartz cells (RF-3010-T) and sealed with a PTFE screw cap inside a glovebox prior to characterization. All spectra were blank subtracted and corrected for scattering of the excitation source. Also, all PL spectra were smoothed with a LOESS function (span of 0.1) after solvent blank and scattering corrections due to the high level of noise introduced from the intense scattering nature of the samples, poor dispersibility, and the fiber-optic-based measurement (in the case of the JAZ).

Single-wavelength Time-correlated Single Photon Counting Measurements

Photoluminescence decays of 0.1 mg mL^{-1} SiNS dispersions in acetonitrile were acquired with a Horiba DeltaFlex time correlated single photon counting fluorimeter. The samples were excited with a 359 nm LED and the decays were collected at a wavelength of 510 nm using a bandpass of 32 nm. In general, the decays were collected for 30 min or until the peak count reached 10k counts, whichever occurred first.

Spectrally and Time-resolved Photoluminescence

Spectrally and time-resolved photoluminescence was measured with a custom-built system at Argonne National Laboratory's Center for Nanoscale Materials. The excitation source was a pulsed (2 kHz) 800 nm Ti : sapphire femtosecond laser (approximate pulse width of 30 fs). For these measurements, the laser frequency was doubled to 400 nm and multiple filters (including neutral density, shortpass, and longpass) were placed in the beam's path to control the laser power, isolate the 400 nm light from the beam, and remove scattering of the excitation source. Additionally, a spot size of approximately 0.5 mm and a power of 5 µW (assessed with a ThorLabs power meter), equating to a fluence of 2.5 uJ cm^{-2}, was employed. The beam was directed to samples mounted on a sapphire substrate with copper tape and the PL was collected through a fiberoptic and directed to a streak camera for detection. The spectrally (301.6 to 793 nm at an interval of ~0.8 nm) and time-resolved data were acquired at four different time windows (5 ns, 50 ns, 2 µs, 20 µs). Data were collected and initially processed with Hamamatsu's HPD-TA software. To obtain the full PL decay, the spectrally resolved counts were integrated as a function of wavelength from 450 to 650 nm and the individual decays at each time window were manually stitched together to yield a single decay from 5 ns to 2 (or 20) µs. To obtain the time-dependent spectral profiles, the spectrally resolved counts (across the entire collection range) were first standardized to exposure number and then converted to counts per second (cps), followed by integration as a function of time from 0.5 to 5 ns, 5 to 50 ns, 0.2 to 2 µs, and 2.4 to 20 µs. Prior to normalization of these spectra, the spectra were smoothed with a LOESS function (span of 0.1) to improve clarity.

Samples for these measurements were prepared as such: piles of powder were placed in a uniform array on a clean sapphire substrate in a nitrogen-filled glovebox. The piles were then covered with copper tape to (i) provide a means to mount the substrate for characterization and (ii) protect them from air exposure during mounting. Data were collected under vacuum to avoid undesirable oxidation of the materials.

Absolute Quantum Yield Measurements

The absolute quantum yield measurements were conducted at Argonne National Laboratory's Center for Nanoscale Materials using an Edinburgh Fluorescence Spectrometer (FLS1000) equipped with an integrating sphere accessory. The SiNS samples were dispersed in ACN in 4 mL quartz cuvettes with screw caps and briefly bath sonicated for 5-10 min prior to immediate data collection. The samples were excited at 400 nm and the PL was monitored between 385 and 800 nm. Slit widths were held constant throughout all measurements. The absolute quantum yield values were calculated with the FLS1000 software.

Structural and Mechanistic Schematics

All presented structures were generated in the free, open-source 3D computer graphics software, Blender™, using the "Atomic Blender (PDB/XYZ)" add-on. Prior to importing the structures into Blender™, the precursor structural files (.cif) were converted to .pdb using the free, open-source molecular editor, Avogadro. For both $CaSi_2$ and the SiNSs, DFT-generated .cif files for 6R-$CaSi_2$ and Si_2H_2 were employed; these files were generated in our previous works.[2,3] In the case of the SiNSs, the Si_2H_2 unit cell was propagated along the a- and b-axes in Avogadro to generate $Si_{30}H_{30}$ before converting to a .pdb file. Once imported in Blender™, the $Si_{30}H_{30}$ surface terminations were manually manipulated to generate $Si_{30}H_{37}Cl_6(OH)_3$, which is equivalent to our previously assessed surface composition of $SiH_{0.7}Cl_{0.2}(OH)_{0.1}$.[4] Note, the periphery of the monolayer was manually terminated with SiH_2 and SiH_3 groups, hence the higher quantity of hydrogen in the generated structure. For all other structures and mechanistic schematics, the base $Si_{30}H_{37}Cl_6(OH)_3$ structure was manually altered in Blender™ to yield the final schematics.

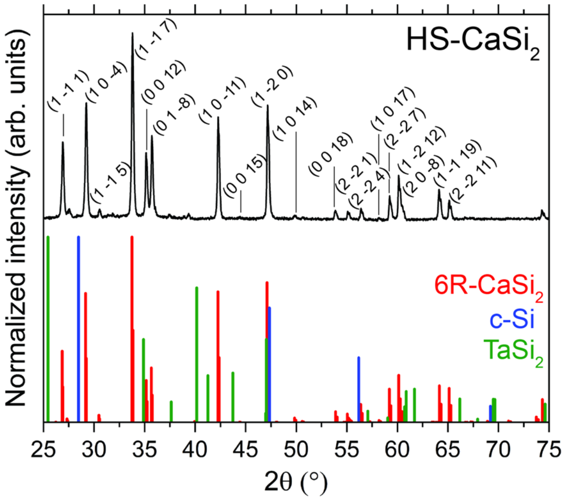

Fig. S1 Representative pXRD pattern of the HS-CaSi$_2$ precursors employed in this work. The reference patterns of 6R-CaSi$_2$ (ICSD entry #32006), as well as common contaminants, bulk silicon (c-Si; COD entry #96-901-3103) and TaSi$_2$ (COD entry #96-153-8770), are provided below to highlight the phase purity of the precursor.

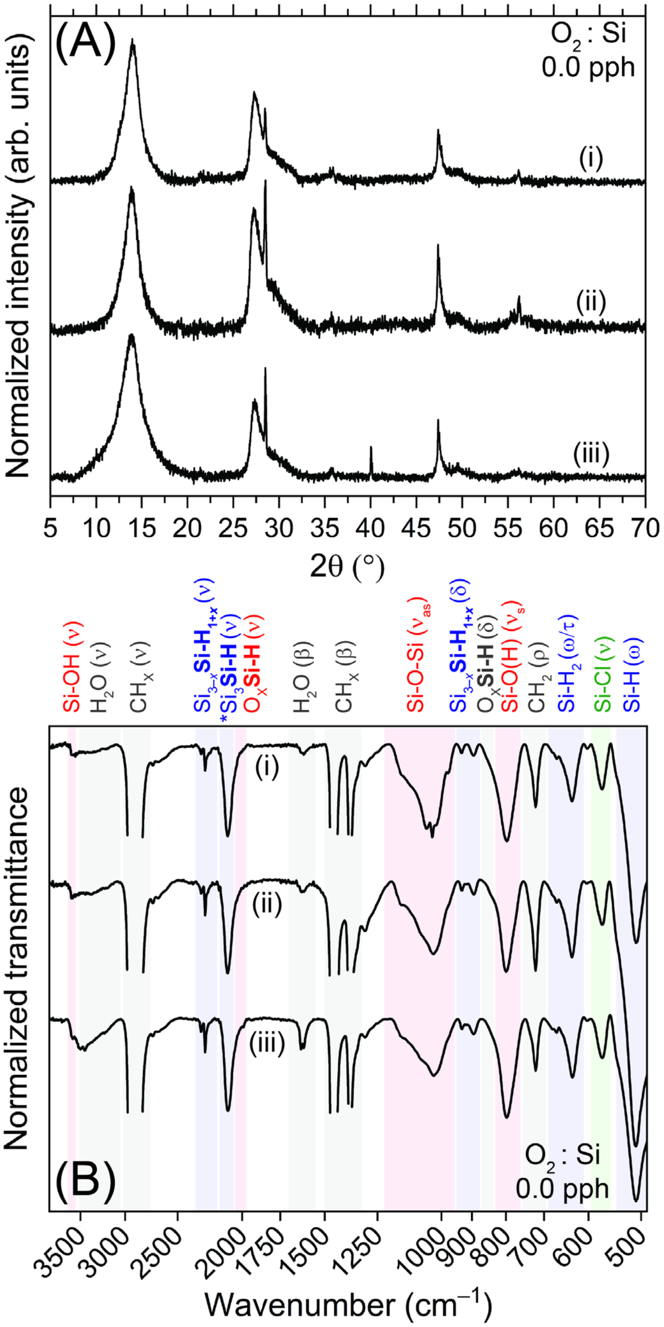

Fig. S2 (A) pXRD patterns and (B) FTIR spectra of three separate SiNS samples prepared in degassed HCl (0.0 pph O_2 : Si) showing the reproducibility of the approach. *Note, all FTIR spectra were normalized to the Si_3Si-H stretch near 2100 cm^{-1}. Also, the most intense CH_x vibrations (originating from oil) were truncated for clarity.

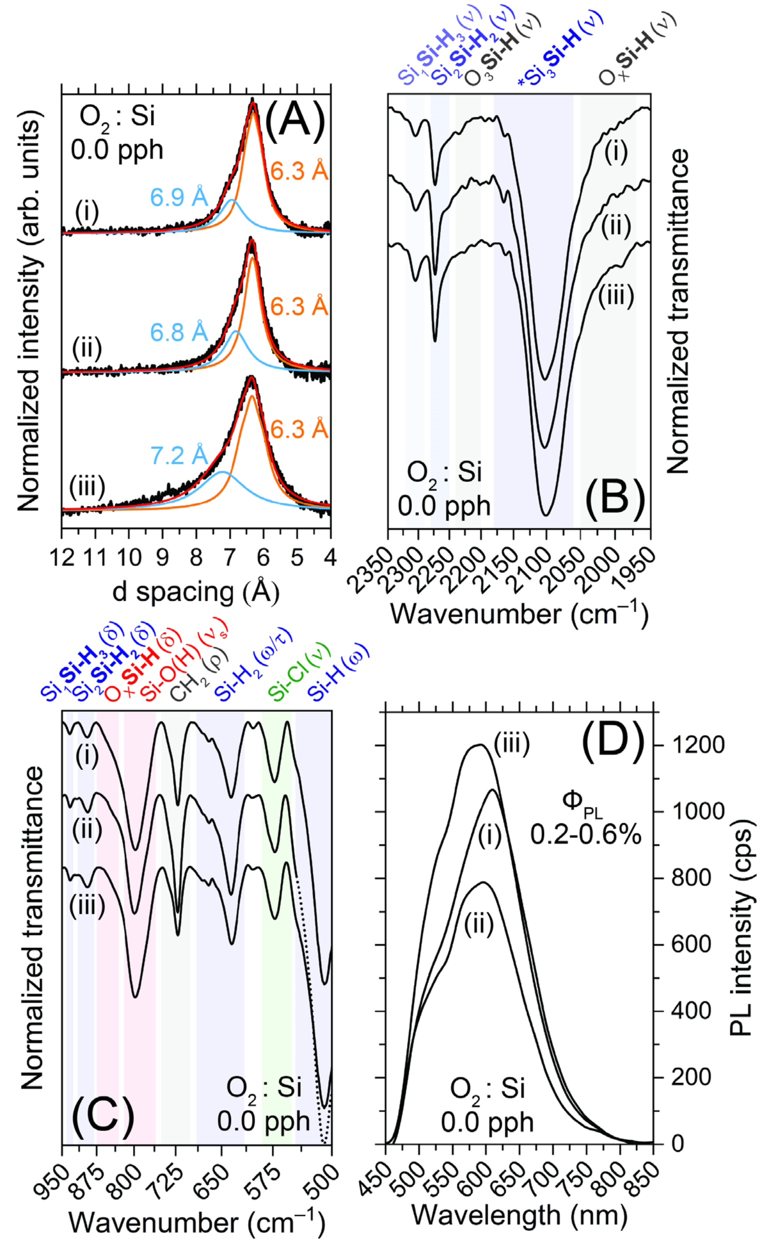

Fig. S3 Reproducibility of SiNSs prepared in degassed HCl (*i.e.*, 0.0 pph O_2 : Si). (A) Deconvoluted pXRD patterns highlighting the consistency in d spacing. The slight shoulders centered near 7 Å arise from slight oxidation. (B and C) FTIR spectra focused on Si-H stretching (panel (B)) and the fingerprint region (panel (C)). *Note, all FTIR spectra were normalized to the Si_3Si-H stretch near 2100 cm^{-1}. Also, the portion of the spectrum for sample (ii) plotted as a dashed line in panel (C) is done so solely for clarity. (D) Steady-state PL spectra of 0.5 mg mL^{-1} ACN dispersions of the SiNSs prepared in degassed HCl. The samples were excited with a 385 nm LED. The absolute PL quantum yield values for these samples ranged from 0.2 to 0.6%.

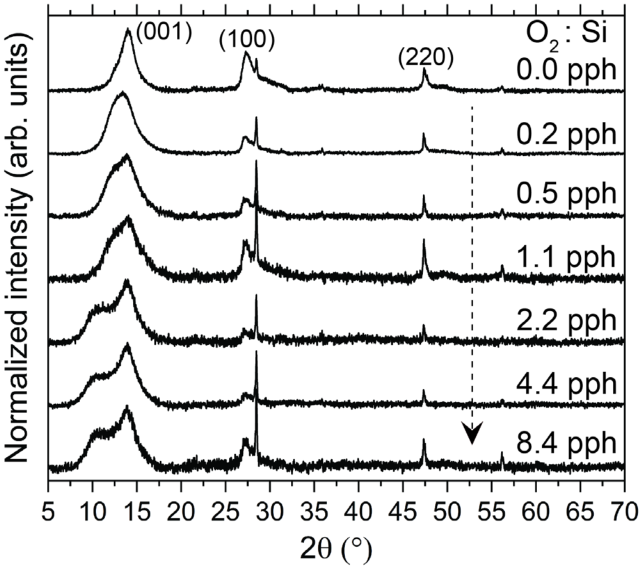

Fig. S4 pXRD patterns of SiNSs prepared in degassed HCl (0.0 pph O_2 : Si) or air-saturated HCl (0.2 pph O_2 : Si), as well as SiNS samples intentionally exposed to dried air (0.5 to 8.4 pph O_2 : Si). The dashed arrow indicates increasing oxygen exposure.

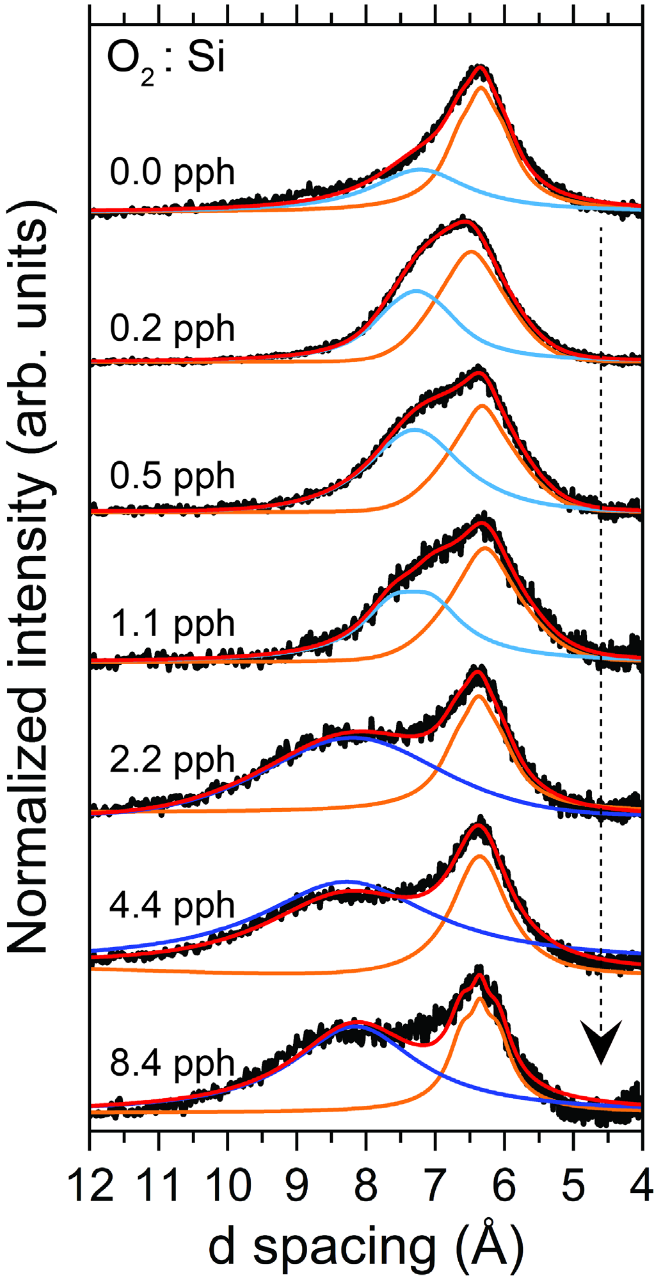

Fig. S5 Deconvoluted pXRD patterns of SiNSs prepared in degassed HCl (0.0 pph O_2 : Si) or air-saturated HCl (0.2 pph O_2 : Si), as well as SiNS samples intentionally exposed to dried air (0.5 to 8.4 pph O_2 : Si). The dashed arrow indicates increasing oxygen exposure.

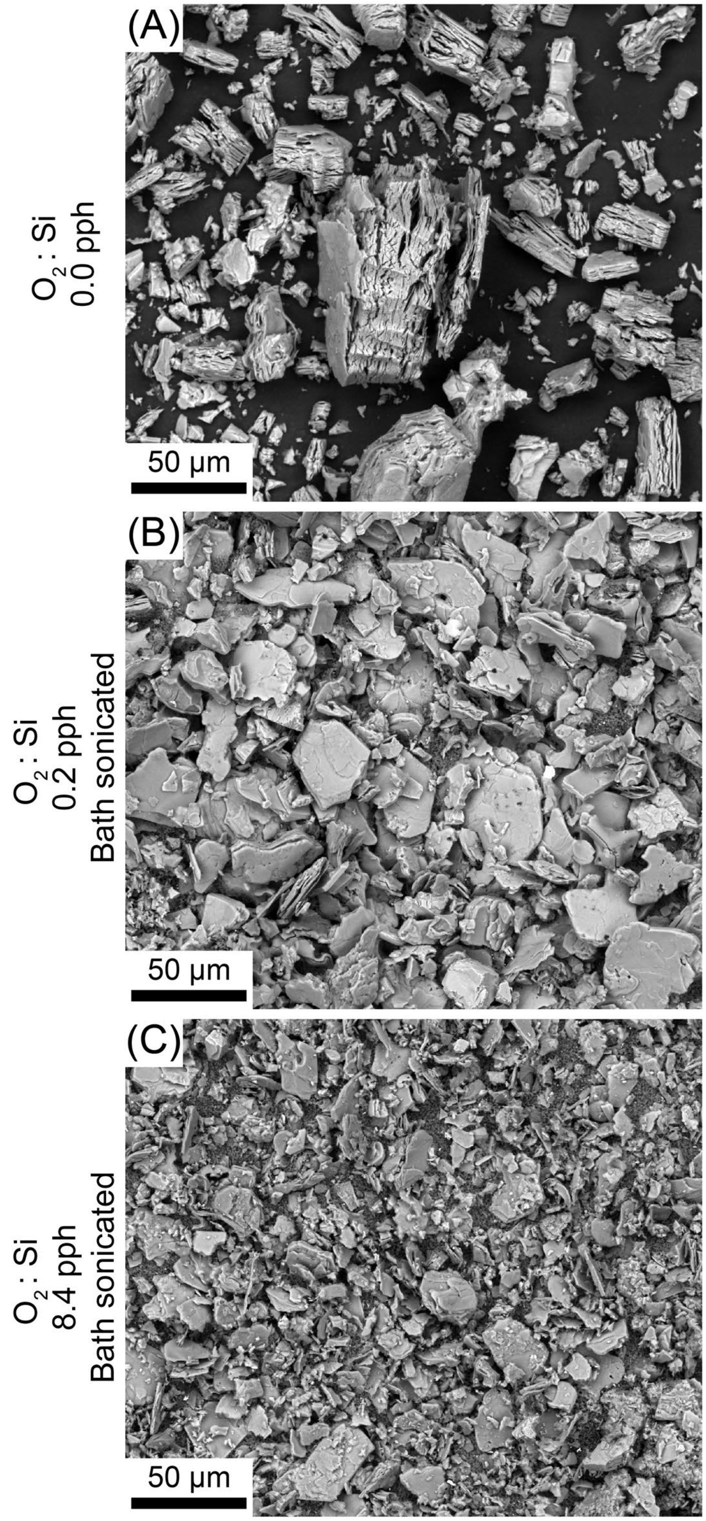

Fig. S6 Representative SEM images of (A) SiNSs prepared in degassed HCl (0.0 pph O_2 : Si), (B) SiNSs prepared in air-saturated HCl (0.2 pph O_2 : Si) and bath sonicated in ACN, and (C) SiNSs bath sonicated and oxidized (by dried air) in ACN. The sample shown in panel (C) is the most oxidized sample explored in this study (8.4 pph O_2 : Si). The apparent size reduction in nanosheet (stack) size is attributed to exfoliation upon bath sonication and not a product of oxidation.

Table S1. Atomic percentages of Si, O, Cl, and Ca, as assessed by EDS. The as-collected values were also adjusted for oxygen originating from the carbon tab and chlorine originating from residual calcium chloride trapped within the nanosheet stacks to verify the measured changes in oxygen and chlorine content could be attributed to alterations of the SiNS chemistry. The uncertainties associated with the values are 99% confidence intervals.

Data treatment	O_2 : Si (pph)	Si	O	Cl	Ca
As-collected	0.0	62.3 ± 1.7	18.2 ± 1.9	17.0 ± 0.5	2.5 ± 0.1
	0.2	66.9 ± 1.7	20.7 ± 1.8	11.4 ± 0.5	1.1 ± 0.1
	0.5	65.8 ± 1.7	25.3 ± 1.5	7.8 ± 0.3	1.1 ± 0.1
	2.2	53.1 ± 1.8	39.6 ± 1.6	6.3 ± 0.4	1.1 ± 0.1
	8.4	50.8 ± 2.3	42.2 ± 2.7	6.0 ± 0.5	1.0 ± 0.1
O from C tab removed	0.0	67.4 ± 1.5	11.4 ± 1.6	18.4 ± 0.4	2.7 ± 0.2
	0.2	73.7 ± 3.0	12.5 ± 3.6	12.6 ± 0.9	1.2 ± 0.1
	0.5	70.0 ± 1.5	20.6 ± 1.4	8.3 ± 0.4	1.1 ± 0.1
	2.2	59.0 ± 2.2	32.9 ± 2.2	7.0 ± 0.4	1.2 ± 0.2
	8.4	57.4 ± 1.0	34.7 ± 1.2	6.8 ± 0.4	1.1 ± 0.1
Residual $CaCl_2$ removed	0.0	73.5 ± 1.6	12.5 ± 1.8	14.1 ± 0.4	—
	0.2	76.5 ± 3.1	13.0 ± 3.7	10.6 ± 0.9	—
	0.5	72.5 ± 1.6	21.3 ± 1.5	6.2 ± 0.4	—
	2.2	61.2 ± 2.2	34.1 ± 2.3	4.7 ± 0.5	—
	8.4	59.4 ± 0.8	35.9 ± 1.4	4.7 ± 0.7	—

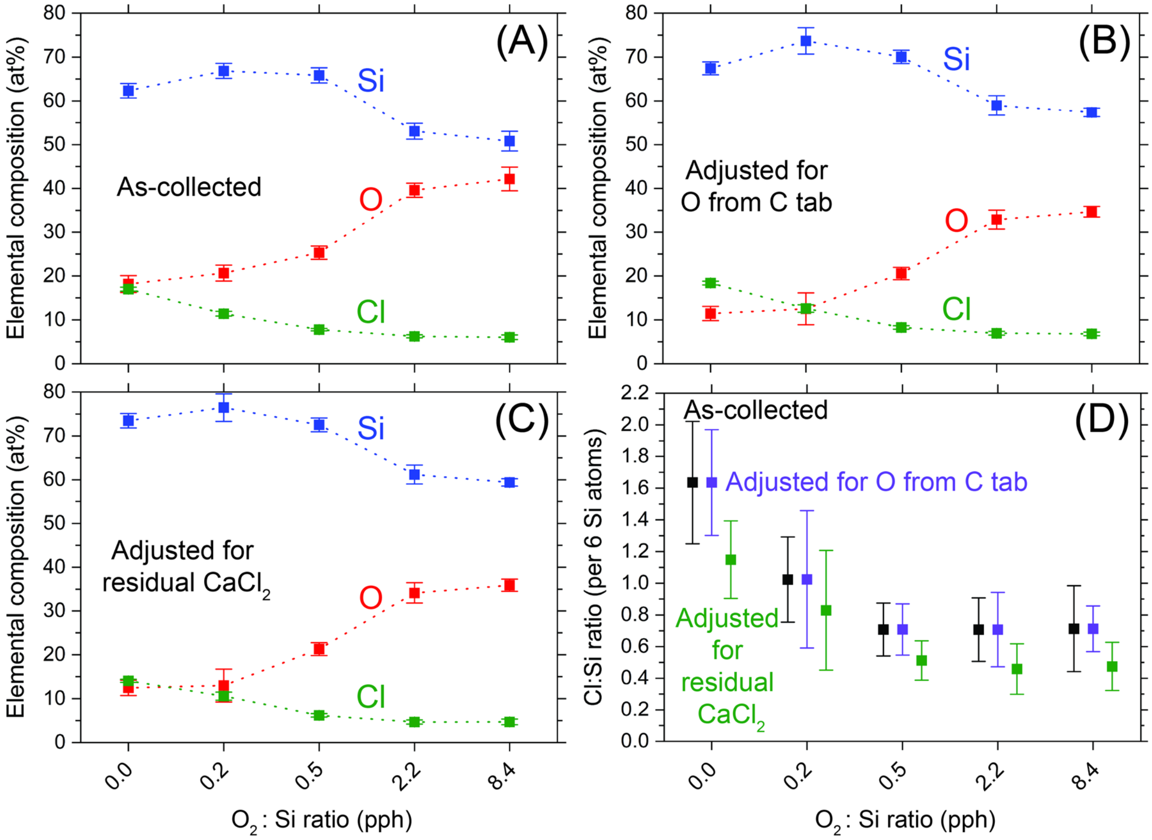

Fig. S7 (A) SiNS elemental composition (at% of Si, O, and Cl), as assessed by EDS. The as-collected values were also adjusted for (B) oxygen originating from the carbon tab and (C) chlorine originating from residual calcium chloride trapped within the nanosheet stacks to verify the measured changes in oxygen and chlorine content could be attributed to alterations of the SiNS chemistry. (D) Cl : Si atomic ratios, in Cl per 6 Si, for the data presented in panels (A)–(C).

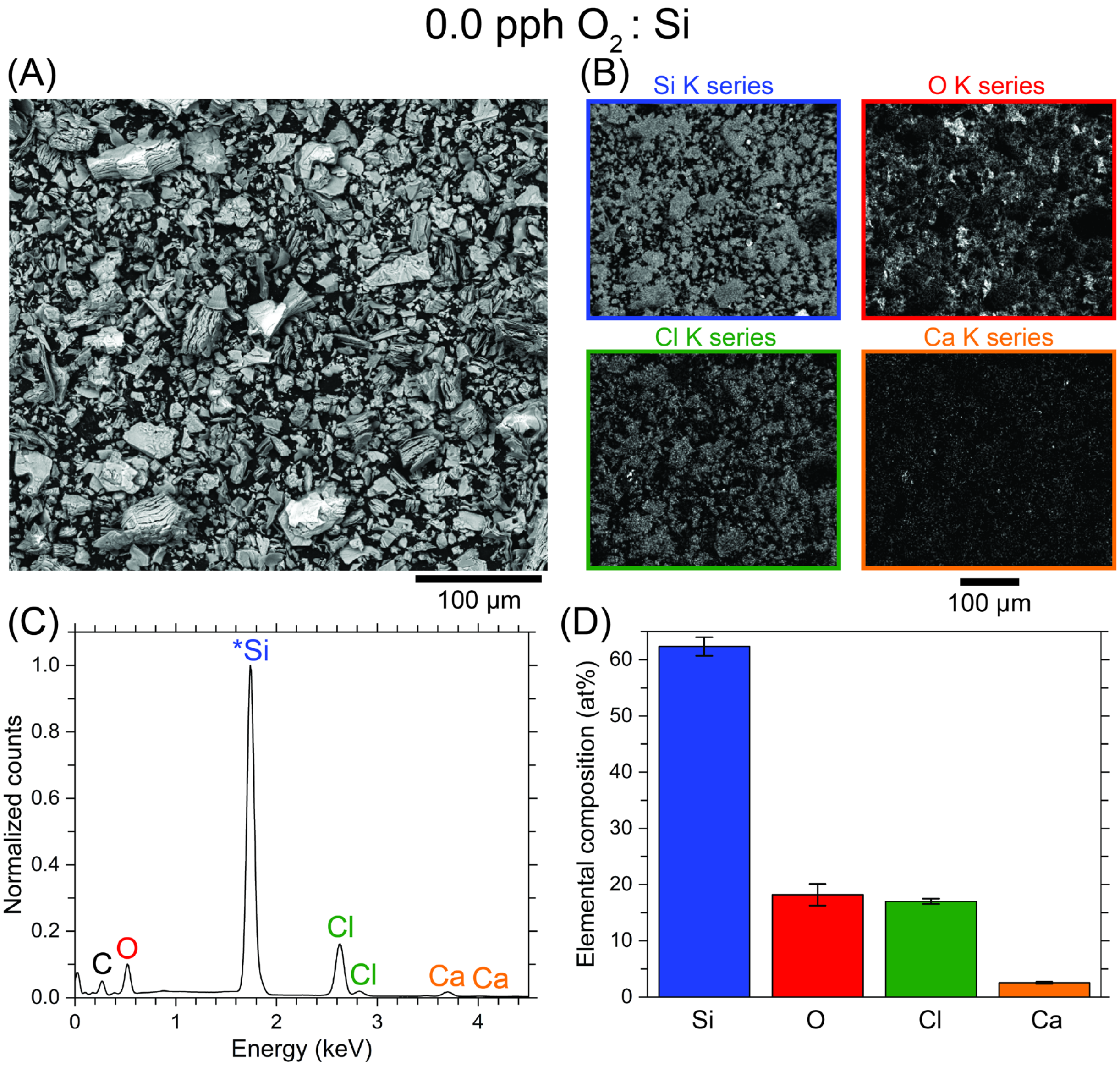

Fig. S8 Representative EDS analysis of SiNSs generated in degassed HCl (0.0 pph O_2 : Si). (A) Backscattered electron image of the area that the elemental maps shown in panel (B) originate from. (C) Average EDS spectrum. The average was assessed from individual EDS spectra of at least three features (*i.e.*, sheet stacks) within a given region, with multiple regions of deposited sample analyzed. *The spectrum was normalized to the Si peak. (D) Average elemental composition of the same features probed in panel (C). The atomic percentages provided are the as-collected values and the error bars represent 99% confidence intervals.

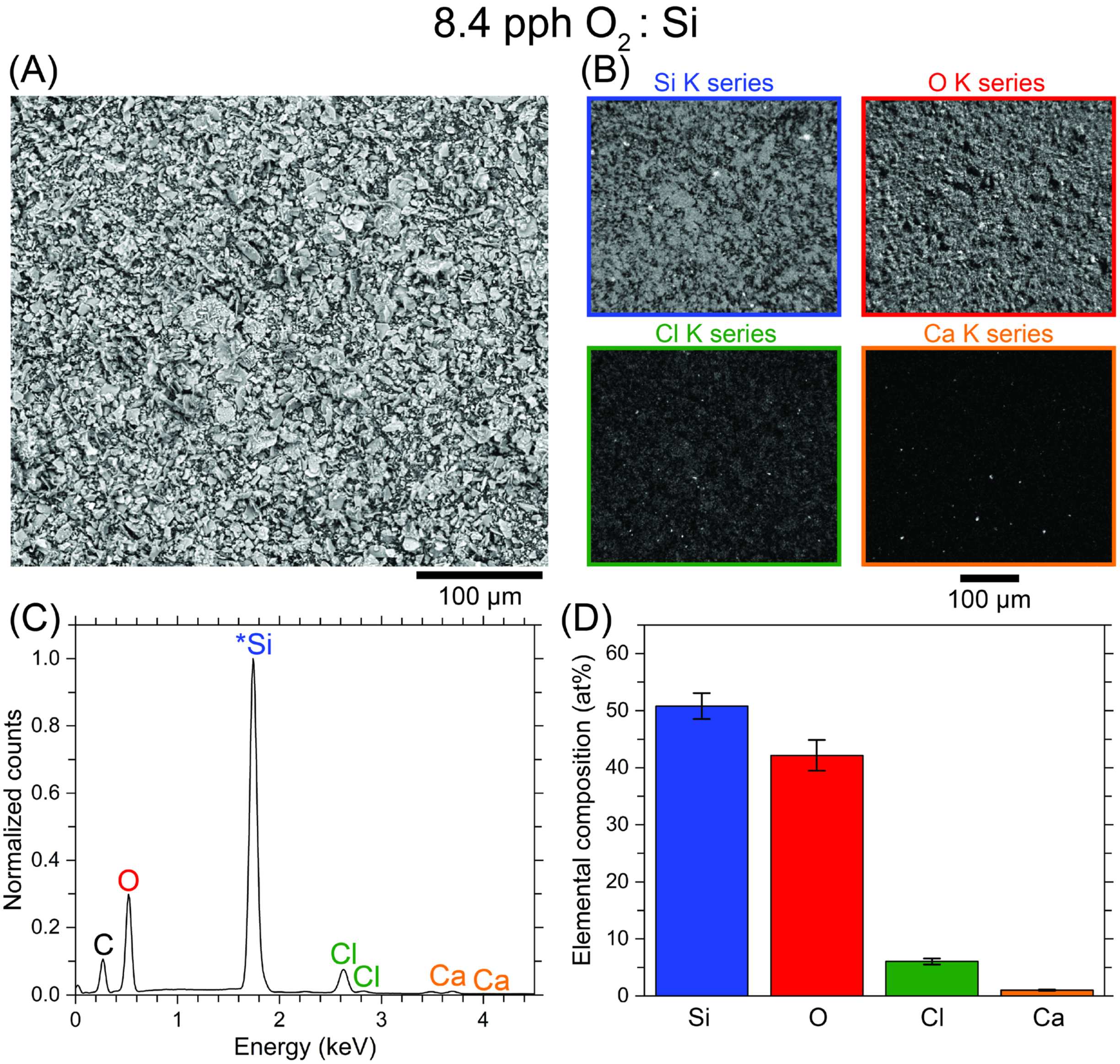

Fig. S9 Representative EDS analysis of SiNSs exposed to the highest quantity of dried air (8.4 pph O_2 : Si). (A) Backscattered electron image of the area that the elemental maps shown in panel (B) originate from. (C) Average EDS spectrum. The average was assessed from individual EDS spectra of at least three features within a given region, with multiple regions of deposited sample analyzed. *The spectrum was normalized to the Si peak. (D) Average elemental composition of the same features probed in panel (C). The atomic percentages provided are the as-collected values and the error bars represent 99% confidence intervals.

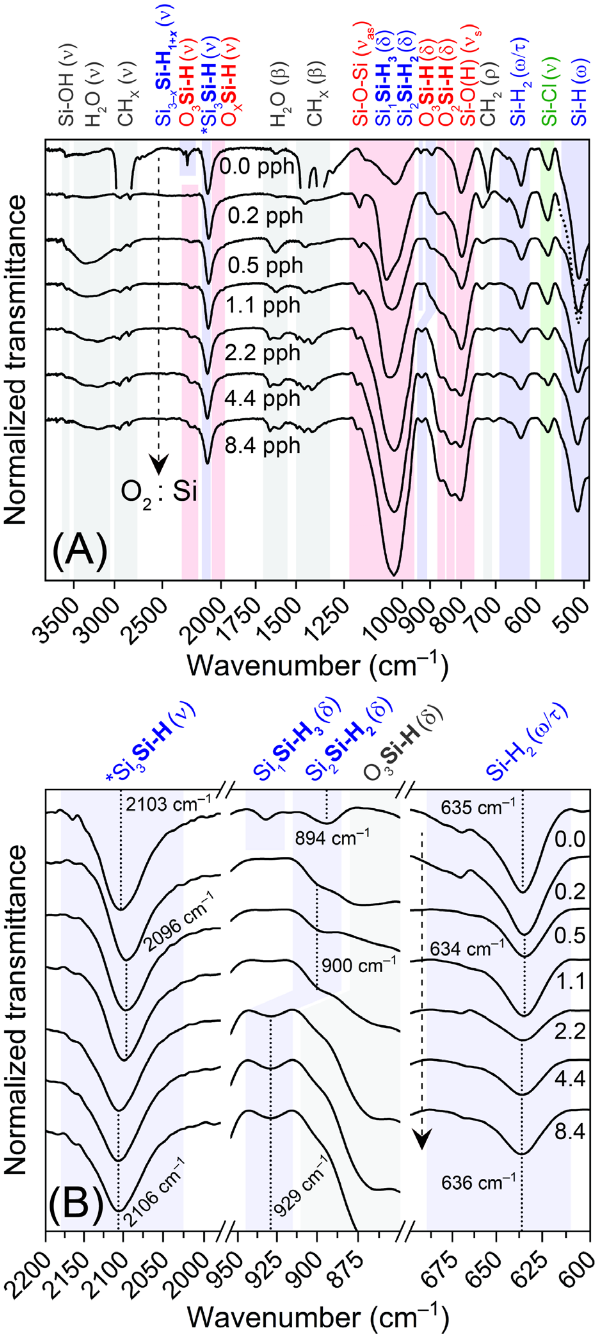

Fig. S10 (A) Full wavenumber range, FTIR spectra of SiNSs prepared in degassed HCl (0.0 pph O_2 : Si; immersed in oil) and air-saturated HCl (0.2 pph O_2 : Si), as well as the oxidized SiNS samples (0.5 to 8.4 pph O_2 : Si). Note, the most intense CH_x vibrations (originating from oil) were truncated and the portion of the spectra for the 0.2 pph O_2 : Si sample was plotted as a dashed line solely for clarity. (B) FTIR spectra shown in panel A focused on Si-H vibrations to highlight trends in spectral shifts upon increasing oxygen exposure. *Note, all FTIR spectra were normalized to the Si_3Si-H stretch near 2100 cm^{-1}. The dashed arrows in both panels indicate exposure to increasing quantities of dried air, while dotted lines are provided to guide the eyes.

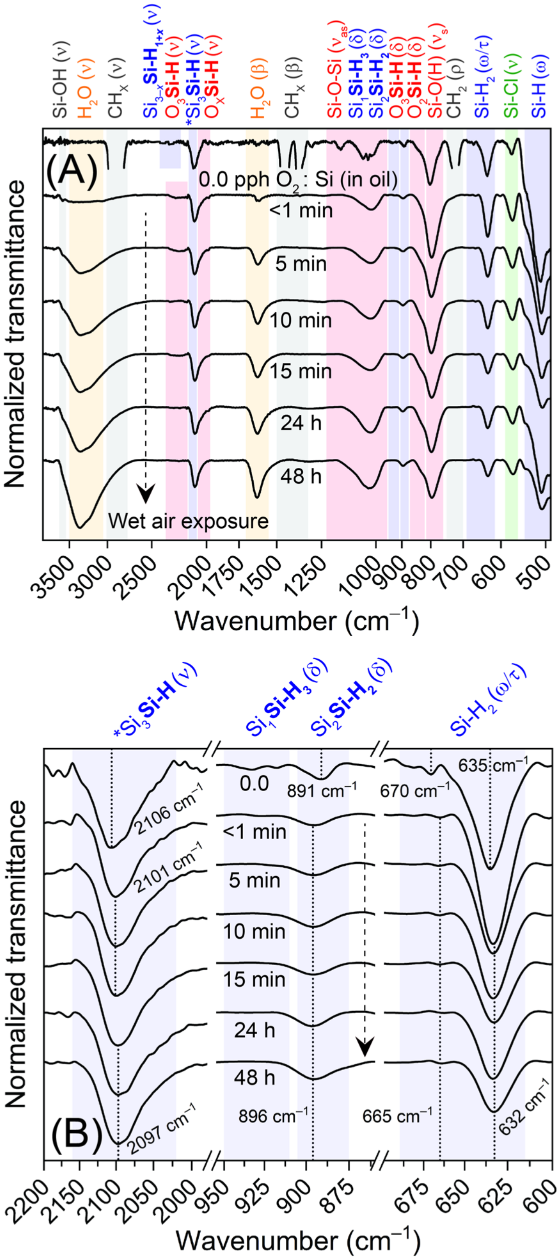

Fig. S11 (A) FTIR spectra of SiNSs prepared in degassed HCl (0.0 pph O_2 : Si; immersed in oil) and the same SiNSs exposed to wet air for the indicated times. Note, the CH_x vibrations were truncated for clarity. (B) FTIR spectra shown in panel A focused on Si-H vibrations to highlight trends in spectral shifts upon increasing air exposure. *Note, all FTIR spectra were normalized to the Si_3Si-H stretch near 2100 cm^{-1}. The dashed arrows in both panels indicate exposure to increasing quantities of dried air, while dotted lines are provided to guide the eyes.

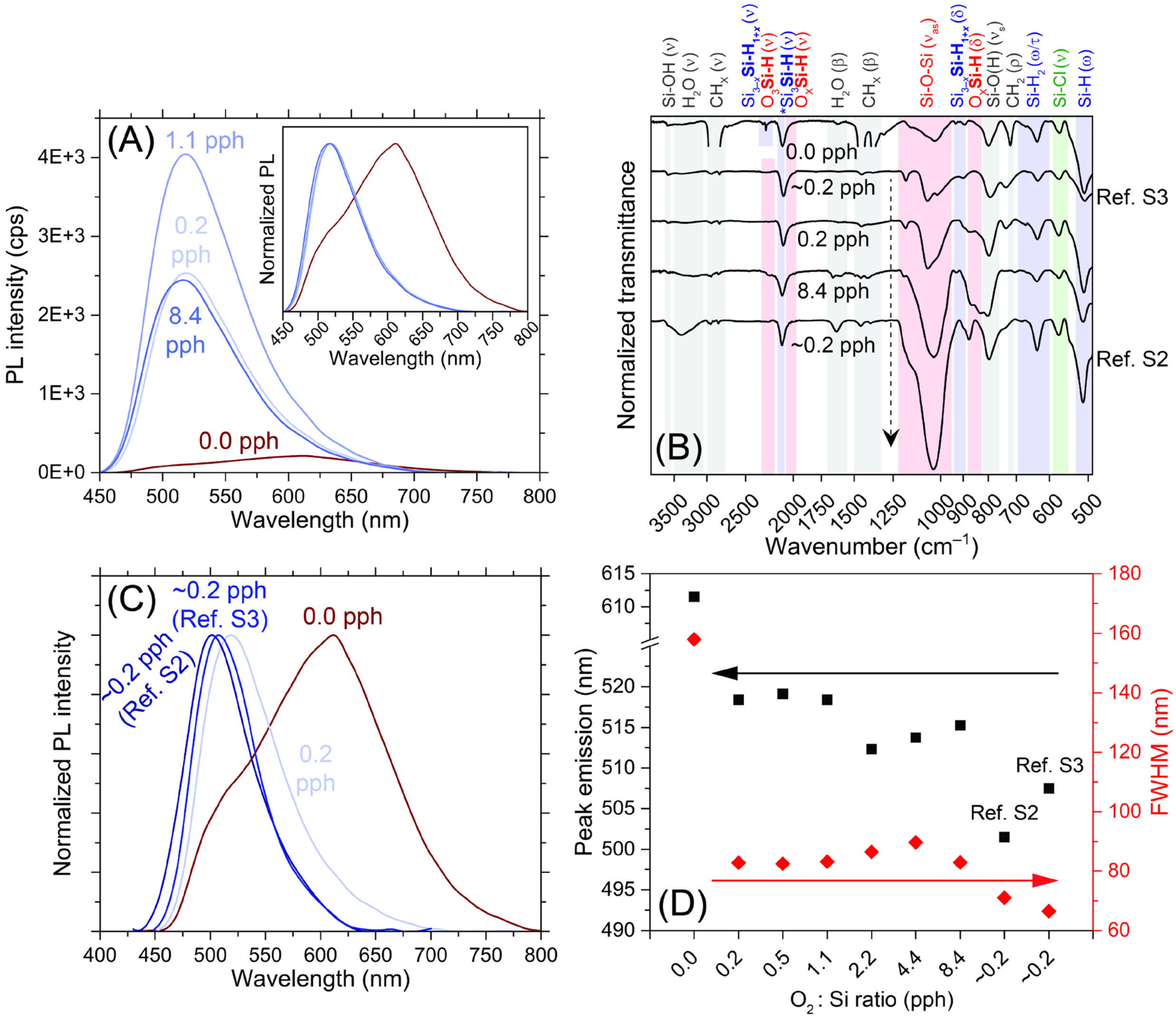

Fig. S12 (A) Steady-state PL for SiNSs exposed to 0.0, 0.2, 1.1, and 8.4 pph O_2. The inset displays the same spectra normalized to their peak maximum to better highlight the differences in spectral profile. (B) FTIR spectra of the 0.0, 0.2, and 8.4 pph O_2 : Si samples generated in this work compared to previously reported SiNSs that were prepared in air-saturated HCl (~0.2 pph); see references S2 and S3. (C) Normalized steady-state PL comparison of 0.0 pph O_2 : Si to different samples prepared in air-saturated HCl (~0.2 pph). (D) Comparison plot of the PL peak and full-width at half maximum from all samples explored in this study and our previously reported SiNS samples.

Table S2. Room temperature TCSPC fitting parameters for the data shown in Fig. S13A. The PL decays were fit to the following tri-exponential function: $I(t) = A_1e^{-t/\tau 1} + A_2e^{-t/\tau 2} + A_3e^{-t/\tau 3}$. The calculated lifetimes are reported in nanoseconds and the preexponential factors (A_1 to A_3) were converted to percent contributions.

O_2:Si ratio (pph)	ACN dispersions			MeOH dispersions		
	τ_1 (A_1)	τ_2 (A_2)	τ_3 (A_3)	τ_1 (A_1)	τ_2 (A_2)	τ_3 (A_3)
~0.2 (Ref. S2)	–	–	–	0.65 ns (87%)	6.3 ns (11%)	61 ns (2%)
0.0	0.60 ns (76%)	4.0 ns (17%)	21 ns (7%)	0.69 ns (86%)	5.5 ns (11%)	58 ns (3%)
0.5	0.97 ns (76%)	6.6 ns (19%)	48 ns (5%)	0.71 ns (90%)	6.1 ns (8%)	46 ns (2%)
1.1	1.0 ns (75%)	6.9 ns (20%)	49 ns (5%)	0.77 ns (86%)	6.4 ns (11%)	41 ns (3%)
2.2	0.98 ns (77%)	5.7 ns (18%)	36 ns (5%)	0.80 ns (85%)	5.8 ns (11%)	26 ns (4%)
4.4	0.92 ns (81%)	5.9 ns (15%)	43 ns (4%)	0.79 ns (87%)	5.4 ns (10%)	27 ns (3%)
8.4	0.87 ns (86%)	6.0 ns (12%)	45 ns (2%)	0.88 ns (81%)	5.6 ns (14%)	24 ns (5%)

Table S3. Room temperature, spectrally resolved TRPL fitting parameters for the data shown in Fig. S13B. PL decays were collected at multiple time windows (5 ns, 50 ns, and 2 μs), stitched together to yield a single PL decay, and the single decay was fit to the following tri-exponential function: $I(t) = A_1e^{-t/\tau 1} + A_2e^{-t/\tau 2} + A_3e^{-t/\tau 3}$. The calculated lifetimes are reported in nanoseconds and the preexponential factors (A_1 to A_3) were converted to percent contributions.

O_2:Si ratio (pph)	Powders		
	τ_1 (A_1)	τ_2 (A_2)	τ_3 (A_3)
0.0	1.1 ns (94%)	16.9 ns (5.6%)	302.5 ns (0.3%)
0.5	1.5 ns (90%)	23.8 ns (9.2%)	319.8 ns (0.8%)
8.4	1.4 ns (91%)	12.1 ns (8.4%)	158.3 ns (0.1%)

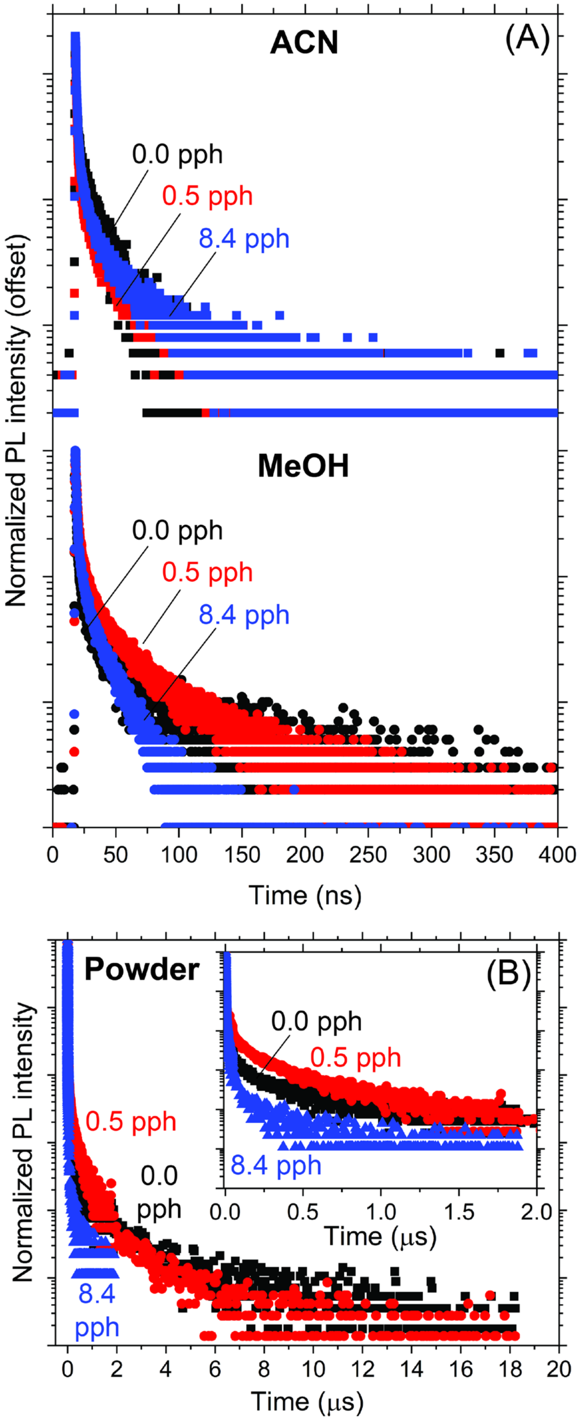

Fig. S13 (A) PL decays of the 0.0, 0.5, and 8.4 pph O_2 : Si samples obtained from TCSPC. The SiNS samples were dispersed in ACN or MeOH at a concentration of 0.1 mg mL^{-1} and the instrument was set at the following conditions: excitation wavelength - 359 nm, emission wavelength - 510 nm, and slit width - 32 nm. (B) PL decays of the 0.0, 0.5, and 8.4 pph O_2 : Si samples obtained from spectrally and time-resolved PL measurements. Decays were collected over multiple time windows (5 ns, 50 ns, 2 μs, 20 μs) and stitched together.

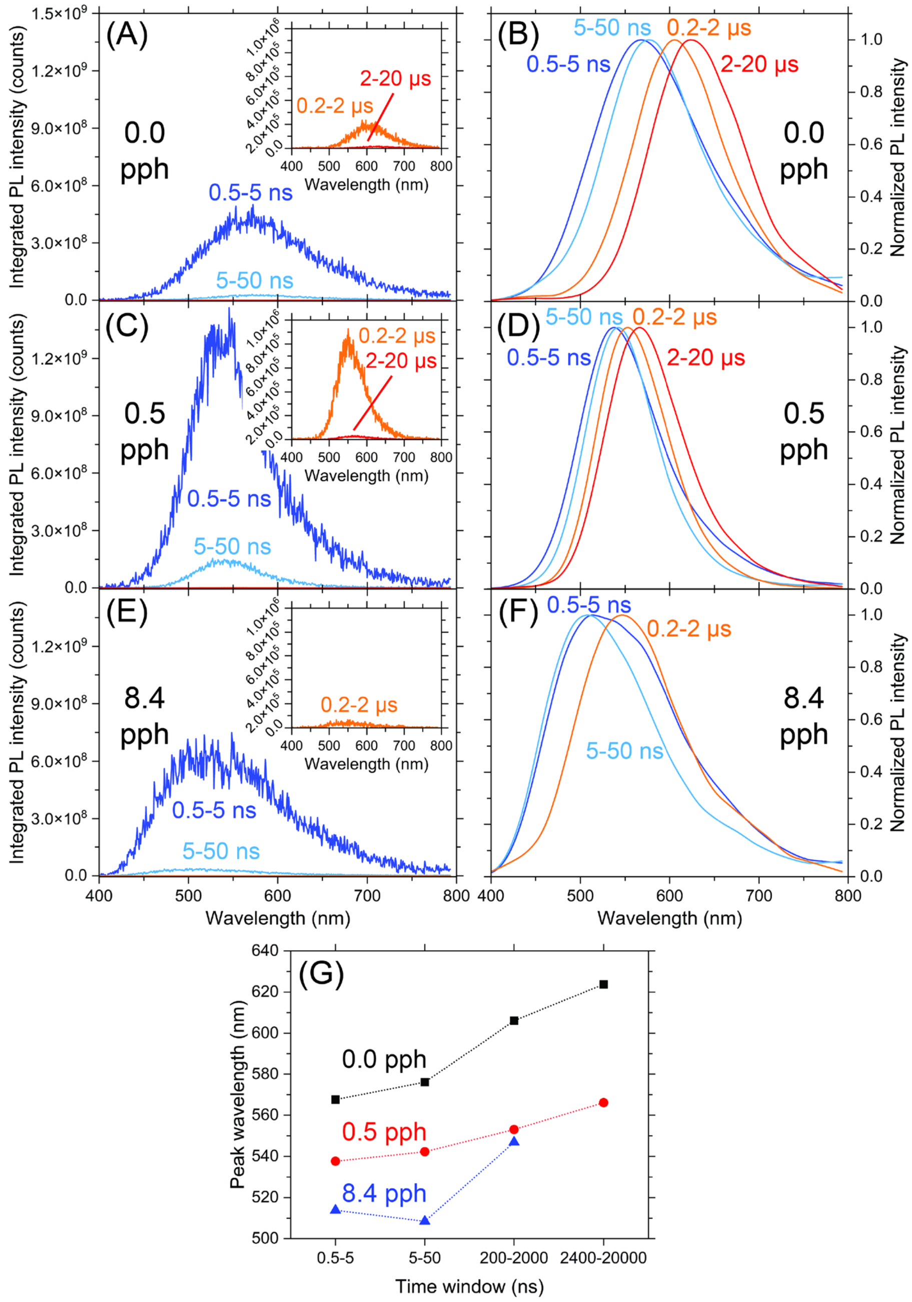

Fig. S14 Time-integrated spectrally resolved counts for the (A) 0.0, (C) 0.5, and (E) 8.4 pph O_2 : Si samples. The insets in panels (A), (C), and € show the longer time windows and have the same y-axis units as the main panels. Respective smoothed and normalized spectra are provided in panels (B), (D) and (F). The spectra were smoothed for clarity to better highlight the observed wavelength shifts as a function of decay time, as shown in panel (G).

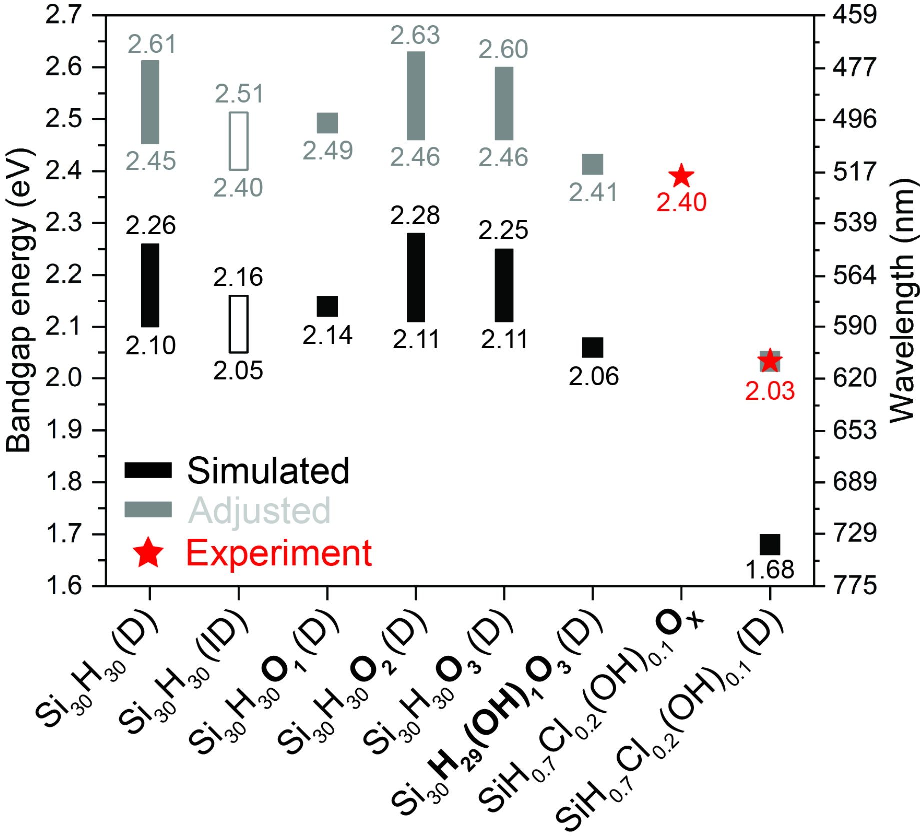

Fig. S15 Comparison of experimentally observed bandgaps for samples generated in this work (red stars) to previously simulated direct (D) and indirect (ID) bandgaps or bandgap ranges reported in the literature for fully hydrogen terminated SiNSs, various oxidized forms of hydrogen terminated SiNSs, and $SiH_{0.7}Cl_{0.2}(OH)_{0.1}$. The simulated values/ranges are the lower energy values shown in black. All previously simulated values were also adjusted by the energy discrepancy (0.35 eV) between the experimental bandgap energy for the non-oxidized SiNSs generated in this work and the previously simulated bandgap energy for $SiH_{0.7}Cl_{0.2}(OH)_{0.1}$. The adjusted values/ranges are the higher energy values shown in gray. This comparison shows that the experimentally observed bandgap energies for oxidized SiNSs (~2.40 eV) line up well with previously simulated bandgap energies for oxidized SiNSs, particularly SiNSs that have three inserted oxygen atoms about a Si containing OH termination ($Si_{30}H_{29}(OH)_1O_3$; 2.41 eV). This similarity in bandgap energy also suggests that oxidation of the Si backbone by molecular oxygen is initiated at and concentrated about Si-OH groups, consistent with our previous report that it is enthalpically favorable for oxygen to attack a Si that already contains Si-O bonds.[3] Note, the simulated ranges were established by pooling simulated bandgap values from references 2–4.

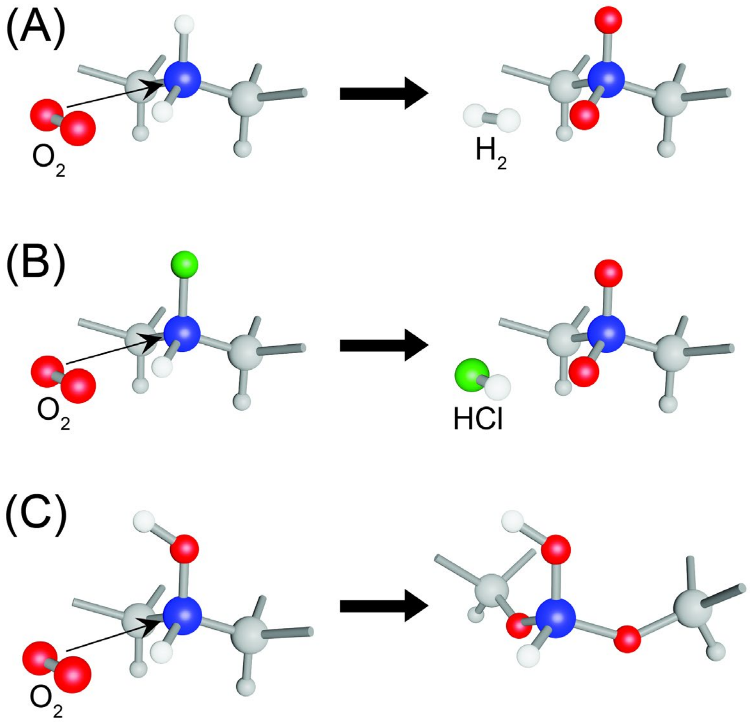

Fig. S16 Schematic representations of potential oxidative pathways in 2D Si showing oxidative attack of (A) SiH_2 edge groups, resulting in the loss of H_2 and the formation of O_2Si, (B) SiH_1Cl_1 edge groups, resulting in loss of HCl and the formation of O_2Si, or (C) $SiH_1(OH)_1$ edge groups, resulting in the formation of O_3Si (in the form of $O_2SiH_1(OH)_1$).

Supporting information references

S1 B. J. Ryan, G. Bhaskar, J. B. Essner, A. Bera, R. W. Dorn, Y. Guo, Q. Hua Wang, A. J. Rossini, J. V. Zaikina, L. T. Roling and M. G. Panthani, *ACS Appl. Nano Mater.*, 2023, **6**, 10054–10063.

S2 B. J. Ryan, M. P. Hanrahan, Y. Wang, U. Ramesh, C. K. A. Nyamekye, R. D. Nelson, Z. Liu, C. Huang, B. Whitehead, J. Wang, L. T. Roling, E. A. Smith, A. J. Rossini and M. G. Panthani, *Chem. Mater.*, 2020, **32**, 795–804.

S3 B. J. Ryan, L. T. Roling and M. G. Panthani, *ACS Nano*, 2021, **15**, 14557–14569.

S4 R. W. Dorn, B. J. Ryan, S. N. S. Lamahewage, M. V Dodson, J. B. Essner, R. Biswas, M. G. Panthani and A. J. Rossini, *Chem. Mater.*, 2023, **35**, 539–548.